

# The Monolayer Thickness Dependence of Quantized Double-Layer Capacitances of Monolayer-Protected Gold Clusters

Jocelyn F. Hicks, Allen C. Templeton, Shaowei Chen,<sup>†</sup> Kevin M. Sheran, Ramesh Jasti, and Royce W. Murray\*

Kenan Laboratories of Chemistry, University of North Carolina, Chapel Hill, North Carolina 27599-3290

Justin Debord, T. Gregory Schaaff, and Robert L. Whetten\*

School of Physics and Chemistry, Georgia Institute of Technology, Atlanta, Georgia 30332-0400

**This report describes how the electrochemical double-layer capacitances of nanometer-sized alkanethiolate monolayer-protected Au clusters (MPCs) dissolved in electrolyte solution depend on the alkanethiolate chain length (C4 to C16). The double-layer capacitances of individual MPCs ( $C_{\text{CLU}}$ ) are sufficiently small (sub-attoFarad, aF) that their metal core potentials change by  $>0.1$  V increments for single electron transfers at the electrode/solution interface. Thus, the current peaks observed are termed “quantized double layer charging peaks”, and their spacing on the potential axis varies with  $C_{\text{CLU}}$ . Differential pulse voltammetric measurements of  $C_{\text{CLU}}$  in solutions of core-size-fractionated (i.e., monodisperse) MPCs are compared to a simple theoretical model, which considers the capacitance as governed by the thickness of a dielectric material (the monolayer, whose chain length is varied) between concentric spheres of conductors (the Au core and the electrolyte solution). The experimental results fit the simple model remarkably well. The prominent differential pulse voltammetric charging peaks additionally establish this method, along with high-resolution transmission electron microscopy and laser ionization–desorption mass spectrometry, as a tool for evaluating the degree of monodispersity of MPC preparations. We additionally report on a new tactic for the preparation of monodisperse MPCs with hexanethiolate monolayers.**

The level of research interest<sup>1</sup> in nanometer-sized metallic and semiconducting particles has increased enormously over the past decade. From a fundamental perspective, there is a tremendous amount of information to be uncovered about this dimension of matter that bridges small molecules and bulk materials. A substantial barrier to its broad exploration has been the dearth of synthetic pathways leading to structurally and compositionally definable nanomaterials. In the case of coinage metal nanopar-

ticles, a seminal step was taken by Schiffrin and co-workers<sup>2</sup> in their synthesis of nanometer-sized alkanethiolate monolayer-protected gold clusters (MPCs). These materials are noteworthy in that they are easy to prepare and are also stable against aggregation when dried of solvent, can be repeatedly isolated and redissolved, and can be functionalized using simple chemical reactions.<sup>3</sup> Our laboratory has contributed to the synthetic elaboration of MPCs as large, polyfunctional molecules.<sup>3,c,d</sup> We<sup>4</sup> and others<sup>5</sup> have also contributed to elucidation of additional properties of MPC monolayers.

The metal cores of MPCs have also experienced substantial investigation and have yielded significant discoveries.<sup>6</sup> For alkanethiolate-protected MPCs, a particularly interesting core property is its sub-attoFarad (aF) capacitance ( $C_{\text{CLU}}$ ) when dissolved in an electrolyte solution. The small MPC capacitance arises from the combination of its tiny radius (0.7–1.0 nm in this work) and the low dielectric of the surrounding hydrocarbon-like monolayer. The consequence of the small capacitance is that single electron transfers to/from the core lead to readily measurable changes ( $\Delta V$ ) in its electronic potential (i.e.,  $\Delta V = [e/C_{\text{CLU}}]$

- (2) Brust, M.; Walker, M.; Bethell, D.; Schiffrin, D. J.; Whyman, R. *J. Chem. Soc., Chem. Commun.* **1994**, 801–802.
- (3) (a) Hostetler, M. J.; Green, S. J.; Stokes, J. J.; Murray, R. W. *J. Am. Chem. Soc.* **1996**, *118*, 4212–4213. (b) Ingram, R. S.; Hostetler, M. J.; Murray, R. W. *J. Am. Chem. Soc.* **1997**, *119*, 9175–9178. (c) Templeton, A. C.; Hostetler, M. J.; Kraft, C. T.; Murray, R. W. *J. Am. Chem. Soc.* **1998**, *120*, 1906–1911. (d) Templeton, A. C.; Hostetler, M. J.; Warmoth, E. K.; Chen, S.; Hartshorn, C. M.; Krishnamurthy, V. M.; Forbes, M. D.; E.; Murray, R. W. *J. Am. Chem. Soc.* **1998**, *120*, 4845–4849. (e) Brown, L. O.; Hutchison, J. E. *J. Am. Chem. Soc.* **1997**, *119*, 12384–12385.
- (4) (a) Hostetler, M. J.; Wingate, J. E.; Zhong, C.-J.; Harris, J. E.; Vachet, R. W.; Clark, M. R.; Londono, J. D.; Green, S. J.; Stokes, J. J.; Wignall, G. D.; Glish, G. L.; Porter, M. D.; Evans, N. D.; Murray, R. W. *Langmuir* **1998**, *14*, 17–30. (b) Hostetler, M. J.; Stokes, J. J.; Murray, R. W. *Langmuir* **1996**, *15*, 3604–3612. (c) Wuelfing, W. P.; Gross, S. M.; Miles, D. T.; Murray, R. W. *J. Am. Chem. Soc.* **1998**, *120*, 12696–12697.
- (5) See, for example: (a) Brust, M.; Fink, J.; Bethell, D.; Schiffrin, D. J.; Kiely, C. *J. Chem. Soc., Chem. Commun.* **1995**, 1655–1656. (b) Leff, D. V.; Ohara, P. C.; Heath, J. R.; Gelbart, W. M. *J. Phys. Chem.* **1995**, *99*, 7036–7041. (c) Badia, A.; Gao, W.; Singh, S.; Demers, L.; Cuccia, L.; Reven, L. *Langmuir* **1996**, *12*, 1262–1269. (d) Badia, A.; Singh, S.; Demers, L.; Cuccia, L.; Brown, G. R.; Lennox, R. B. *Chem. Eur. J.* **1996**, *2*, 359–363. (e) Badia, A.; Cuccia, L.; Demers, L.; Morin, F.; Lennox, R. B. *J. Am. Chem. Soc.* **1997**, *119*, 2682–2692. (f) Wang, Z. L.; Harfenist, S. A.; Whetten, R. L.; Bentley, J.; Evans, N. D. *J. Phys. Chem. B* **1998**, *102*, 3068–3072.

<sup>†</sup> Present address: Department of Chemistry, Southern Illinois University, Carbondale, IL 62901-4409.

(1) (a) Schmid, G. *Clusters and Colloids. From Theory to Applications*; VCH: New York, 1994. (b) Haberland, H., Ed. *Clusters of Atoms and Molecules*; Springer-Verlag: New York, 1994.

$> k_B T$ , where  $e$  is the electronic charge). That is, electrochemical charging of the MPC core becomes a quantized process. The effect is formally analogous to classical STM-based “Coulomb staircase” experiments,<sup>6f–i</sup> and has also been seen with nanometer-sized electrodes.<sup>7</sup>

A scan of electrode potential in an MPC solution leads to a series of diffusion-controlled<sup>6g</sup> current features, observable as waves in microelectrode voltammetry<sup>6h</sup> and as peaks in macroelectrode differential pulse and cyclic voltammetry.<sup>6f–i</sup> The disposition of these current peaks on the potential axis reflects the underlying nature of the MPC core charging process. If the metal core is sufficiently small ( $< \text{ca. } 100$  atoms) as to develop molecule-like properties, an electrochemical band gap (analogous to an optical band gap) appears<sup>6g</sup> as a wide spacing between the two current peaks adjacent to the MPC potential of zero charge ( $E_{\text{PZC}}$ ). If on the other hand, the MPC core is large enough to be metal-like, the band gap disappears, the current peaks become more regularly spaced, and the charging becomes an electrostatic phenomenon, which in the electrochemical context is called double-layer charging. Our previous papers<sup>6f–i</sup> referred to this first as “ensemble Coulomb staircase” charging, but more recently by the simpler name “quantized double-layer charging”. The electrochemical current peaks described here will be termed quantized double-layer (DL) peaks.

It is the purpose of this paper to further explore our designation of the observed current peaks as double layer charging phenomena, by measuring their spacing for MPCs with varied alkanethiolate monolayer chain length and by comparing the resulting  $C_{\text{CLU}}$  values to a simple electrostatic capacitor model, that of concentric spheres. The model was additionally inspected through  $C_{\text{CLU}}$  measurements of C6 chain length MPCs in solvents of differing dielectric constant. The simple model (described later), although approximate in a number of ways, represents the data remarkably well.

Observation of current peaks for quantized DL charging requires that the MPCs in the solution have reasonably uniform values of  $C_{\text{CLU}}$ ; unresolved overlapping of differently spaced current peaks would otherwise lead to a featureless charging background. A uniform  $C_{\text{CLU}}$  translates to uniform MPC core radius and monolayer thickness and composition. As prepared MPCs from the Brust reaction<sup>2</sup> are normally somewhat polydisperse in core size (seen in transmission electron microscopy, TEM), and fractionation is required to procure monodisperse MPC

samples. Fractionation has been described for C4 and C6 MPCs (and confirmed by laser ionization–desorption mass spectrometry<sup>6a</sup>), but not for longer chain length alkanethiolate MPCs. Fractionation of the latter is made difficult by the increasingly similar solubilities of MPCs of large and small core size, when the core is covered with thicker monolayers, but is accomplished here for C8, C10, C12, and C16 MPCs. Fractionation of C6 MPCs is also found to be facilitated by use of an extraction (as opposed to precipitation<sup>6a</sup>) procedure. Characterization of progress in fractionation requires a size-sensitive analytical tool; differential pulse voltammetry (DPV) is demonstrated to have the needed sensitivity, by comparison to mass spectrometric and TEM results.

It is useful to understand that the consecutive (one-electron) double layer charging peaks of MPC solutions are *formally* analogous to current peaks seen in traditional redox reactions. That is, the quantized DL charging currents are diffusion controlled<sup>6g</sup> (by the mass transport of the MPCs), and mixtures of MPCs with adjacent states of core charge ( $Z$ ) are mixed-valent solutions that follow the Nernst equation in regard to the *average* core potential. Thus, the potentials at which quantized DL charging events occur are described by<sup>6h</sup>

$$E^{\circ}_{\text{ZZ-1}} = E_{\text{PZC}} + (Z - 1/2)e/C_{\text{CLU}} \quad (1)$$

where  $E^{\circ}_{\text{ZZ-1}}$  is the formal potential of the  $Z/(Z - 1)$  charge state “couple” and is given by DPV peak potentials,  $E_{\text{PZC}}$  is the potential of zero charge (i.e.,  $Z = 0$ ) of the cluster, and  $Z$  is signed such that  $Z > 0$  and  $Z < 0$  correspond to core “oxidation” and “reduction” respectively. This relation predicts a linear plot of  $E^{\circ}_{\text{ZZ-1}}$  vs charge state (termed a “Z-plot”) and is useful in allowing evaluation of an average value of  $C_{\text{CLU}}$  from its slope and inspection for irregular or systematic changes in  $C_{\text{CLU}}$  as a function of potential and charge state. Values of  $C_{\text{CLU}}$  can also, of course, be obtained from the spacing of any adjacent pair of charging peaks, and this has been done previously for those spanning the working electrode PZC which has been estimated<sup>6g</sup> at ca.  $-0.2$  V vs Ag/AgCl in toluene/ $\text{CH}_3\text{CN}$  solvent.

## EXPERIMENTAL SECTION

**Chemicals.** Monolayer-protected clusters (MPCs) with butanethiolate, hexanethiolate, octanethiolate, decanethiolate, dodecanethiolate, and hexadecanethiolate monolayers were prepared using a modification of the Brust reaction.<sup>2,4</sup> Briefly, a 3:1 thiol: Au ratio was employed in all reactions and addition of reductant ( $\text{NaBH}_4$ ) was performed at  $0^\circ\text{C}$ . Following addition of reductant and stirring at room temperature for 24 h, the solvent was removed under vacuum and the crude MPC product collected on a frit where it was washed with copious amounts of ethanol and acetone. The cluster products are abbreviated according to chain length as C8 MPCs, etc. (This population gives a 28 kDa peak in laser desorption–ionization mass spectrometry; another peak seen at 22 kDa corresponds to  $\sim\text{Au}_{116}$ .) Alkanethiols smaller than butanethiol (i.e., propanethiol) could not be used, the derived MPCs being poorly stable.<sup>4a</sup>

**MPC Fractionation.** MPC preparations were fractionated so as to isolate their dominant smaller core size population, which is primarily cores of 145 Au atoms protected with ca. 50 alkanethiolate ligands.<sup>4</sup> The fractionation is based on the greater

(6) (a) Whetten, R. L.; Khoury, J. T.; Alvarez, M. M.; Murthy, S.; Vezmar, I.; Wang, Z. L.; Stephens, P. W.; Cleveland, C. L.; Luedtke, W. D.; Landman, U. *Adv. Mater.* **1996**, *8*, 428–433. (b) Schaaf, T. G.; Shafiqullin, M. N.; Khoury, J. T.; Vezmar, I.; Whetten, R. L.; Cullen, W. G.; First, P. N.; Gutierrez-Wing, C.; Ascensio, J.; Yose-Yacamm, M. J. *J. Phys. Chem. B* **1997**, *101*, 7885–7891. (c) Vezmar, I.; Alvarez, M. M.; Khoury, J. T.; Salisburry, B. E.; Whetten, R. L. *Z. Phys. D* **1997**, *40*, 147. (d) Luedtke, W. D.; Landman, U. *J. Phys. Chem.* **1996**, *100*, 13323–13329. (e) Terrill, R. H.; Postlethwaite, T. A.; Chen, C.-H.; Poon, C.-D.; Terzis, A.; Chen, A.; Hutchison, J. E.; Clark, M. R.; Wignall, G.; Londono, J. D.; Superfine, R.; Falvo, M.; Johnson, C. S.; Samulski, E. T.; Murray, R. W. *J. Am. Chem. Soc.* **1995**, *117*, 12537–12548. (f) Ingram, R. S.; Hostetler, M. J.; Murray, R. W.; Schaaff, T. G.; Khoury, J. T.; Whetten, R. L.; Bigioni, T. P.; Guthrie, D. K.; First, P. N. *J. Am. Chem. Soc.* **1997**, *119*, 9279–9280. (g) Chen, S.; Ingram, R. S.; Hostetler, M. J.; Pietron, J. J.; Murray, R. W.; Schaaff, T. G.; Khoury, J. T.; Alvarez, M. M.; Whetten, R. L. *Science* **1998**, *280*, 2098–2101. (h) Chen, S.; Murray, R. W.; Feldberg, S. W. *J. Phys. Chem. B* **1998**, *102*, 9898–9907. (i) Chen, S.; Murray, R. W. *Langmuir* **1987**, *3*, 682–689. (j) Pietron, J. J.; Hicks, J. F.; Murray, R. W. *J. Am. Chem. Soc.* **1999**, *121*, 5565–5570.

(7) Fan, F.-R. F.; Bard, A. J. *Science* **1997**, *271*, 1791.

solubility in polar solvent mixtures exhibited by MPCs with smaller cores.<sup>6a</sup>

**Precipitation.** Fractionations were performed by incremental precipitation<sup>6a</sup> of larger MPCs from a toluene solution by adding a more polar solvent. A typical procedure starts with ca. 100 mg of as-prepared MPC in toluene (15 mg/mL); this can be scaled up. Addition of an equal volume (7.5 mL) of acetone causes some precipitation; after 24 h this mixture was centrifuged (Fisher Scientific, 1800 rpm) for 30 min and carefully decanted; the ~40 mg insoluble fraction is designated cut A. The soluble fraction was rotovaped to dryness, it was redissolved in toluene at a higher concentration (30 mg/mL), and an equal volume (3.5 mL) of acetone was added, again inducing some precipitation. After waiting 24 h, centrifuging (30 min), and decanting, the insoluble fraction (~20 mg) was collected as cut B. The previous step was repeated on the soluble fraction except that now 2 parts acetone was added to the MPC toluene (30 mg/mL) solution; the insoluble fraction resulting was designated cut C (~30 mg). This was again repeated except that 3 parts acetone was added to the MPC toluene (30 mg/mL) solution; the insoluble fraction (~10 mg) resulting was designated cut D. A further repetition using 4 parts acetone produced an insoluble fraction designated cut E. In practice, the above steps were followed until insufficient material was left for a further precipitation step; in some experiments cut C represented the final insoluble fraction, whereas for a few samples a cut D or cut E could be obtained.

**Extraction.** A newer procedure, which has been successful for C6 MPCs, relies on extraction of as-prepared material with a polar solvent. After stirring of the raw C6 MPC reaction mixture for 24 h, the water layer was removed and the MPC-containing toluene layer rotovaped until all toluene was removed (unreacted thiol, disulfide byproduct, and a small amount of water/borohydride were still present) and an MPC slurry remained. Approximately 200 mL of absolute ethanol was added to the MPC slurry. The solution was covered and allowed to stand for 24 h, after which it was poured through a medium-porosity frit and washed with ca. 30 mL of both acetone and ethanol. The filtrate was then rotovaped to dryness, resuspended in acetonitrile, collected on a frit, and rinsed with an additional 100 mL of acetonitrile. This material (yield ca. 10% of the original amount of cluster) is designated the ethanol-soluble fraction. The ethanol-insoluble fraction was subjected to precipitation fractionation as described above to recover additional 28 kDa MPC sample not extracted. Optimization of the extraction procedure is in progress to remove all of the smaller core size MPCs.

**Measurements.** <sup>1</sup>H NMR spectra (~40 mg of MPC/mL in C<sub>6</sub>D<sub>6</sub>) were recorded on a Bruker AMX 200 MHz NMR spectrometer with a spectral line broadening of 1 Hz to improve signal-to-noise (S/N) resolution. A relaxation delay of 5 s was used to allow adequate signal decay between pulses.

Laser desorption–ionization mass spectra were obtained on a custom-built LDI time-of-flight mass spectrometer (1.2 m).<sup>6a,f</sup> Films of neat MPC were cast (from toluene solutions, 3 mg of MPC/mL) on steel rod tips. After drying under vacuum, the rods were inserted into the ion-source region and irradiated by the unfocused output of a frequency-doubled Nd:YAG laser ( $\lambda = 532$  nm, PW = 5 ns) at a pulse fluence of 20 mJ/cm<sup>2</sup>. The mass spectra shown are for negatively charged particles in which a 15 kV initial

acceleration and a 30 kV post-flight acceleration are employed prior to impact on a conversion-type detector. Digitized TOF wave forms were averaged, calibrated against those of biomolecule standards in the 10–60 kDa range, corrected for desorption ejection velocity, and then converted to mass spectra.

Transmission electron microscopy (TEM) was conducted with a side-entry Phillips CM12 electron microscope operating at 120 keV. TEM samples were prepared by evaporating a drop of ca. 2 mg/mL hexane MPC solution on Formvar-coated (200–300 Å) copper grids (400 mesh). Phase-contrast images of the MPCs were obtained of two typical regions on each sample, at either 340000× or 430000×. Histograms of the Au core sizes were obtained from a digitized photographic enlargement using Scion Image Beta Release 2 (available at www.scioncorp.com).

Differential pulse voltammetry (DPV) was performed with a BAS 100B electrochemical analyzer on degassed ~0.1 mM MPC solutions in either 2:1 (v:v) toluene/CH<sub>3</sub>CN or CH<sub>2</sub>Cl<sub>2</sub> (0.05 M Bu<sub>4</sub>NClO<sub>4</sub> electrolyte), in sealed single-compartment cells containing 1.6 mm diameter Au working, Pt coil counter, and Ag wire quasi-reference (Ag/QRE) electrodes. The working electrode was polished with 0.25 μm diamond (Buehler) paste, rinsed with NANOpure water and successively sonicated in absolute ethanol, acetone, and NANOpure water. The electrode surface was further cleaned by potential cycling (–0.5 to 1.4 V) in 0.5 M sulfuric acid for 2–3 min.<sup>8</sup> Background DPVs (solvent + electrolyte) were taken prior to each experiment to check for spurious waves and excessive background currents, in which case the electrode was recleaned.

## RESULTS AND DISCUSSION

**The Concentric Sphere Capacitance Model.** A capacitor formed from concentric conducting spheres separated by a dielectric (the alkanethiolate monolayer) of thickness  $d$  and static dielectric constant  $\epsilon$  has a capacitance given by<sup>6h</sup>

$$C_{\text{CLU}} = 4\pi\epsilon_0\epsilon(r/d)(r + d) \quad (2)$$

where  $C_{\text{CLU}}$  is the cluster capacitance,  $\epsilon_0$  the permittivity of free space,  $\epsilon$  the dielectric constant of the monolayer,  $r$  the radius of the core, and  $d$  the chain length of the monolayer. Inspection of eq 2 indicates that core radius ( $r$ ) and monolayer chain length ( $d$ ) are the manipulable MPC variables influencing individual cluster capacitances. The cluster capacitance increases with core radius and decreases with monolayer chain length.

The approximations involved in our application of eq 2 to MPCs are stated here more completely than done previously.<sup>6h</sup> First, the MPC core is not thought to be spherical, but instead truncated octahedral, based on theoretical calculations of equilibrium structures.<sup>6a</sup> The average core radius can be directly measured by TEM. Second, an *effective* dielectric constant of  $\epsilon = 3.0$  is used in the comparisons to data; actual values for, say, pentane and pentanethiol monomers would be 1.8 and 4.55. Choices of different values of  $\epsilon$  simply scale capacitances calculated from eq 2 and—unless  $\epsilon$  actually varies with alkanethiolate chain length—would not produce the trend in capacitance expected from changing chain length ( $d$ ). We will show that the experimental  $C_{\text{CLU}}$  is

(8) Woods, R. In *Electroanalytical Chemistry*; Bard, A. J., Ed.; Marcel Dekker: New York 1980; Vol. 9, p 1.

relatively insensitive to the solvent employed, so assuming that  $\epsilon$  does not vary with chain length seems reasonable. Third, the lengths of fully extended alkanethiolate chains are assumed to define  $d$ , the dielectric thickness. Folding of short chains (where  $d < r$ ) leads to prediction of appreciably larger capacitances from eq 2, whereas folding of longer chains (where  $d > r$ ) has a smaller effect on predicted  $C_{\text{CLU}}$ . The extended chain picture is probably most valid for short chain length alkanethiolate (C4, C6) monolayers since the radial dilution of chain density is least at shorter chain lengths. For longer chain lengths, there is a variety of evidence for monolayer disorganization; this evidence includes vibrational spectroscopy of methylene stretches,<sup>4b</sup> modeling of <sup>13</sup>C NMR chemical shifts,<sup>5e</sup> and hydrodynamic radii measurements<sup>3a,b,9</sup> that are consistent with the monolayer behaving as a soft (rather than hard) sphere. Since eq 2 becomes less sensitive to the actual chain length when  $d > r$ , it is difficult to be certain about the presence or absence of partial folding of longer chains.

A fourth assumption of eq 2 is that the spherical monolayer/electrolyte solution interface is sharp and that the electrolyte solution is a good conductor over the entire sphere (i.e., no discreteness of ionic charge effects). Aside from its strong radial character, the monolayer/electrolyte solution interface should be analogous to that on flat electrodes covered with a self-assembled monolayer.<sup>10</sup> The potential drop in the diffuse layer is ignored, and the distance of closest approach of the electrolyte ion's charge to the MPC core is presumed to be the distance  $d$  (the electrolyte ion is treated as a point charge by assuming that  $d =$  the alkanethiolate chain length). These issues are hard to address at this stage of study of quantum DLs; experiments such as varying the electrolyte concentration and use of electrolyte ions calculated to "adsorb" on the MPC surface have not been started.

Finally, we would observe that as with any new phenomenon being experimentally scrutinized, the quality of the data (i.e., exactness of measured  $C_{\text{CLU}}$ ) should improve over time. Thus, effects of some of the above assumptions may be transparent in the present data, but become revealed as data are obtained in a more refined manner.

**Quantum Double-Layer Charging Results.** Differential pulse voltammetry (DPV) is shown in Figure 1 for solutions of fractionated C6, C8, and C12 MPCs in 2:1 toluene/CH<sub>3</sub>CN. The quantum DL charging features are well-defined and, for the C8 and C12 cases, are the first observed for longer chain MPCs, reflecting the grudging success of the precipitation fractionation procedure originally employed for shorter chain materials. (The  $\Delta E_{\text{PEAK}}$  differences seen between the positive and negative-going  $E_{\text{DC}}$  potential scans are attributed mainly to uncompensated resistance losses ( $iR_{\text{UNC}}$ ), although some effect of electron-transfer dynamics is conceivably present.) The DPV curves in Figure 1 show that peak spacing and thus  $C_{\text{CLU}}$  changes regularly with monolayer chain length, as anticipated. For example, the C12 MPC has a larger peak spacing ( $\Delta V = 0.38$  V) and correspondingly smaller capacitance (0.40 aF), relative to the C6 sample ( $\Delta V = 0.27$ ,  $C_{\text{CLU}} = 0.72$  aF).

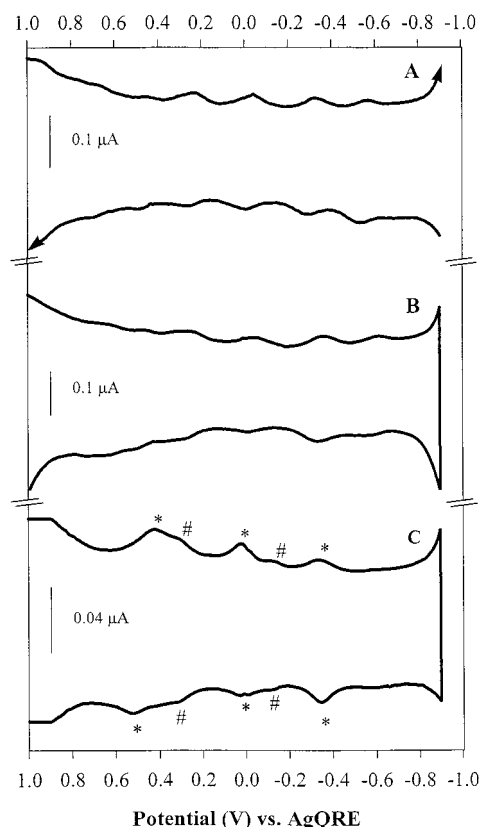


Figure 1. Differential pulse voltammograms (DPVs) showing charging events for ca. 0.1 mM fractionated Au MPCs in 2:1 toluene/CH<sub>3</sub>CN at a 0.5 mm diameter Au working electrode (0.05 M Bu<sub>4</sub>NClO<sub>4</sub>, potential versus Ag QRE reference, Pt coil counter electrode). All charging events shown are above background. (A) C6 MPC cut C; (B) C8 cut D; (C) C12 cut D. The asterisks represent charging events of a 28 kDa MPC, and the number signs are charging events of a 22 kDa sample.

Plots of the Figure 1 peak potentials versus charge state are shown in Figure 2. The corresponding evaluated capacitances as well as those of other chain lengths are presented in Table 1, upper ("full" Z-plot results). Also given in Table 1 are values of  $C_{\text{CLU}}$  calculated from eq 2 using the assumptions noted above, along with associated (extended chain)  $d$  values and core radii ( $r$ ) from TEM or LDI/MS experiments. Repeated capacitance measurements suggest the uncertainty in  $C_{\text{CLU}}$  is ca.  $\pm 0.03$  aF. Comparison of the experimental to calculated values ("ratio") shows that eq 2 represents the 5-fold variation in  $d$  and the ca. 2-fold variation in  $C_{\text{CLU}}$  remarkably well for such a simple model.

Equation 1 suggests that exact values of  $E_{\text{PZC}}$  can be obtained from Z-plots, but data like Figure 2 show that the  $Z = 0$  intercept is not very reproducible, for reasons that are unclear.

DPV experiments were performed in a variety of solvents. Experiments in dichloromethane (DCM) using C6, C8, and C10 MPC samples are shown in Figure 3, the corresponding "Z-plots" in Figure 4, and  $C_{\text{CLU}}$  results in Table 1, lower. Again the experimental and calculated capacitances agree quite well. These observations parallel those of Porter et al.,<sup>10</sup> who found that capacitances of alkanethiolate monolayers of varied chain length on planar Au surfaces changed as expected (except for short chains) for a parallel plate capacitor model.

Table 2 presents measurements of C6 MPC quantized DL charging peaks in five additional solvents. The choices of solvents

(9) (a) Green, S. J.; Stokes, J. J.; Hostetler, M. J.; Pietron, J. J.; Murray, R. W. *J. Phys. Chem. B* **1997**, *101*, 2663–2668. (b) Green, S. J.; Pietron, J. J.; Stokes, J. J.; Hostetler, M. J.; Vu, H.; Wuelfing, W. P.; Murray, R. W. *Langmuir* **1998**, *14*, 5612–5619.  
(10) Porter, M. D.; Bright, T. B.; Allara, D. L.; Chidsey, C. E. D. *J. Am. Chem. Soc.* **1987**, *109*, 3559.

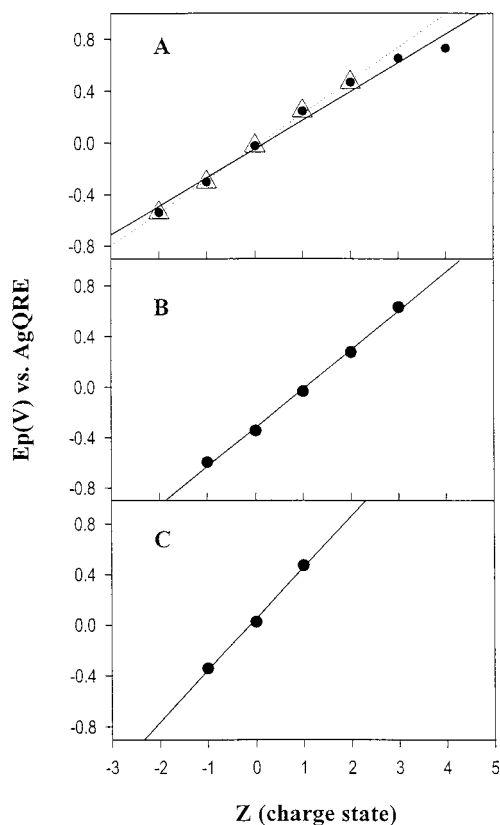


Figure 2. Formal potentials of charging events versus cluster charge state ( $Z$ ), taking  $E_{PZC} \approx -0.2$  V, for C6 (curve A), C8 (curve B), and C12 (curve C). (●) potentials of all charge states plotted (linear regression, —); (Δ) only charge states  $-2$  to  $+2$  plotted (linear regression, ---). Potentials plotted are those for peaks in Figure 1.

Table 1. Cluster Capacitance as a Function of Monolayer Chain Length<sup>a</sup>

chain length ( $r, d, b$ nm)	calcd $C_{CLU}$ , aF	expt $C_{CLU}$ , aF, $Z$ -plots full	slope for $Z = \pm 2^c$	ratio <sup>d</sup> (expt/calcd)
In 2:1 Toluene/ $CH_3CN$				
C4 (0.8, <sup>e</sup> 0.52)	0.69	0.59	0.66	0.9
C6 (0.8, <sup>e</sup> 0.77) <sup>g</sup>	0.53	0.57	0.51	1.1
C6 (1.0, <sup>f</sup> 0.77) <sup>g</sup>	0.77	0.72	0.63	1.1
C8 (0.7, <sup>f</sup> 1.02)	0.40	0.52		1.3
C10 (0.8, <sup>f</sup> 1.27)	0.44	0.47		1.1
C12 (0.8, <sup>e,f</sup> 1.52)	0.39	0.40		1.0
C16 (0.8, <sup>f</sup> 2.52)	0.36	0.39 <sup>f</sup>		1.1
In $CH_2Cl_2$				
C6 (0.8, <sup>h</sup> 0.77) <sup>g</sup>	0.53	0.57	0.5 <sup>g</sup>	1.1
C6 (1.0, <sup>f</sup> 0.77) <sup>g</sup>	0.77	0.70	0.62	1.1
C8 (0.7, <sup>f</sup> 1.02)	0.40	0.55		1.4
C10 (0.8, <sup>f</sup> 1.27)	0.44	0.53		1.2

<sup>a</sup> Clusters are fractionated by precipitation unless otherwise noted and are  $Au_{145}$  (28 kDa) cores. <sup>b</sup> ( $r, d$ ) are core radii obtained from LDI/MS or TEM, and extended chain length obtained from molecular modeling data (Hyperchem). <sup>c</sup>  $Z$ -plot slope taken for  $Z = \pm 2$ ; see Figure 2A. <sup>d</sup> Ratio of full  $Z$ -plot  $C_{CLU}$  to calculated  $C_{CLU}$ . <sup>e</sup> Measured by LDI/MS. <sup>f</sup> Measured by TEM. <sup>g</sup> These are different preparations of the same material made and fractionated by different workers. <sup>h</sup> Ethanol-soluble cluster fraction. <sup>i</sup> See supplemental information for corresponding DPV and  $Z$ -plot.

were determined by joint MPC and electrolyte solubility considerations.  $C_{CLU}$  values were compared to that in the toluene/ $CH_3CN$  solvent mixture. Equation 2 predicts a linear dependence of  $C_{CLU}$  on the monolayer dielectric constant. Table 2 shows that  $C_{CLU}$  is

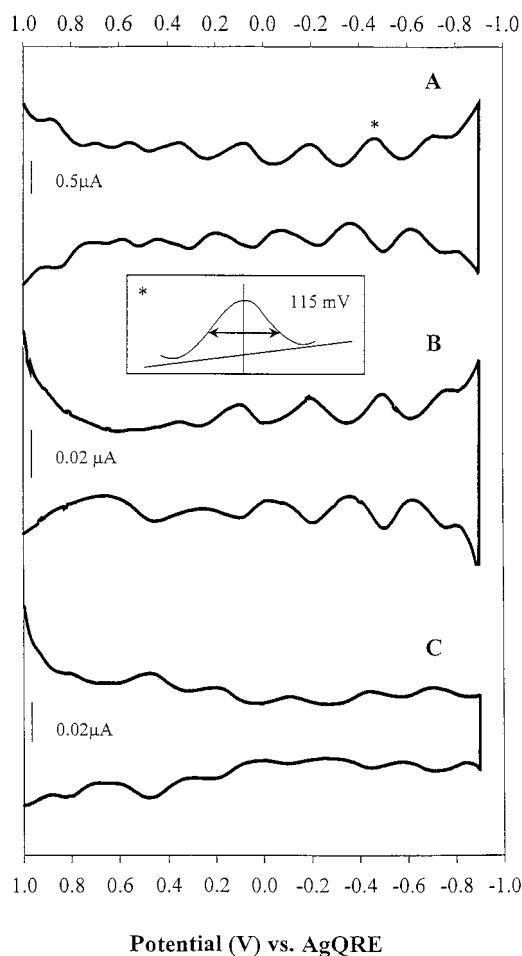


Figure 3. Differential pulse voltammograms (DPVs) showing charging events for ca. 0.1 mM fractionated Au MPCs in dichloromethane (DCM) at a 1.6 mm diameter Au working electrode (0.05 M  $Bu_4NClO_4$ , potential versus Ag QRE reference Pt coil counter electrode). All charging events shown are above background. (A) C6 MPC cut E; (B) C8 MPC cut D; (C) C10 MPC cut D. Inset shows that peak \* on expanded scale has fwhm = 115mV.

relatively constant over a range of nearly 3-fold in solvent dielectric constant. If the solvent, by permeation into the monolayer, were to be a major determinant of the effective value of  $\epsilon$  in the monolayer, substantial variation in  $C_{CLU}$  should occur. It follows that for C6 chain lengths in MPCs, the monolayer properties dominate the effective dielectric constant and in turn the double-layer capacity and  $C_{CLU}$ . Again, the correspondence of the experimental results to the simple model of eq 2 is rather remarkable.

There are, however, as is obvious to the careful reader, features in the above data that are not exactly in accord with eq 2. We collect discussion of these as a group because they seem not to reflect a general but rather isolated, specific (and thus also interesting) divergences. First, the points in  $Z$ -plots for DPV charging peaks of shorter chain MPCs (e.g., Figures 2a and 4a) tend to diverge at the most positive potentials; i.e., the effective value of  $C_{CLU}$  increases there. Exclusion of the two most positive data points from the  $Z$ -plots lowers the experimental  $C_{CLU}$  results (Table 1), but it is difficult to say whether this produces a better agreement with the calculated  $C_{CLU}$ . (The change in  $\Delta V$  at positive potentials is confined to the shorter chain MPCs; it is not seen

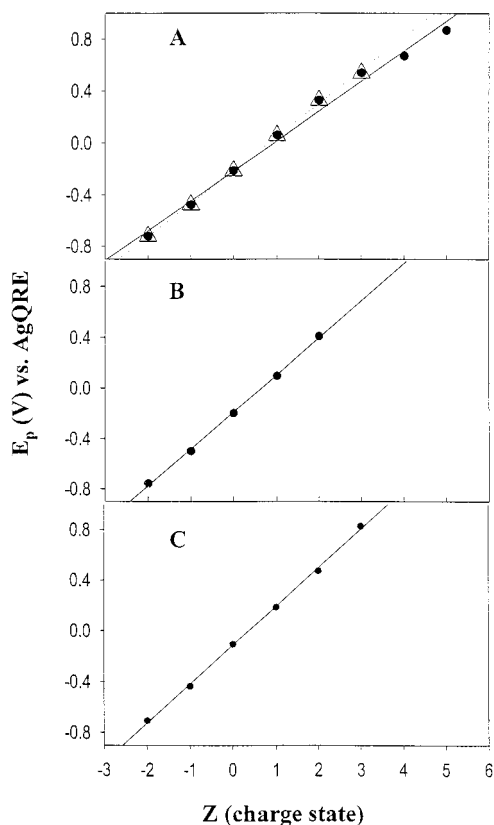


Figure 4. Formal potentials of charging events versus cluster charge state ( $Z$ ): Plots for C6 MPC (A), C8 MPC (B), and C10 MPC (C). (●) Potentials of all charge states plotted (linear regression, —); (Δ) only charge states  $Z = -2$  to  $+3$  plotted (linear regression, ---). Potentials plotted are those shown in Figure 3.

Table 2. C6 MPC Capacitance Measurements in Various Solvents<sup>a</sup>

solvent	dielectric constant ( $\epsilon_s$ )	$C_{CLU}$ , aF	ratio <sup>b</sup>
2:1 toluene/ $\text{CH}_3\text{CN}$	14.1 <sup>c</sup>	0.63 <sup>d</sup>	1.0
pyridine	12.40	0.67	0.9
3:1 toluene/ $\text{CH}_3\text{CN}$	11.5 <sup>c</sup>	0.62	1.0
1,2-dichloroethane	10.4	0.73	0.9
dichloromethane	9.00	0.62	1.0
tetrahydrofuran	7.58	0.66	0.9
chlorobenzene	5.53	0.45 <sup>e</sup>	1.3

<sup>a</sup>All measurements were performed at a 1.6 mm diameter Pt working electrode in 0.30 mM C6 MPC solutions in 0.05 M  $\text{Bu}_4\text{NClO}_4$  electrolyte/solvent. The same MPC sample was recovered and used for all experiments. <sup>b</sup>“Ratio” is capacitance values relative to that measured in 2:1 toluene/ $\text{CH}_3\text{CN}$ . <sup>c</sup>Estimated from pure solvent  $\epsilon_s$  based on volume fractions. <sup>d</sup>A different C6 MPC sample from that reported in Table 1 for the same solvent/electrolyte combination. The difference in capacitance may be attributed to differences in average core size and sample dispersity. <sup>e</sup>DPV charging peaks were observable only at negative potentials for this sample, which may have caused this capacitance value to be underestimated.

for the longer chain MPCs either because it is absent or because the smaller number of charging peaks observable there makes detecting the change difficult.) The origin of the reproducible positive potential  $Z$ -plot divergence in Figures 2a and 4a has not been established; one possibility is electrolyte ion penetration (e.g., specific adsorption of  $\text{ClO}_4^-$ ) into the monolayer at high positive core potential. Porter and co-workers<sup>10</sup> also suggested electrolyte

ion penetration into short chain length monolayers as the source of larger than expected capacitance results.

Second, there are obvious differences in the definition of the DPV peaks in Figures 1 and 3; they are better defined (larger relative to background) in Figure 3 ( $\text{CH}_2\text{Cl}_2$ ) and in both figures at negative potentials. As illustrated in the Figure 3 inset, the average full width half-maximum (fwhm) of a DPV peak in the C6 sample (A) in  $\text{CH}_2\text{Cl}_2$  material can be as small as 115 mV; it should ideally be 90 mV for a reversible one-electron process.<sup>11</sup> The higher measured value could arise from slow electron transfer kinetics (unlikely for a tunneling barrier as short as C6 chain) or, more likely, from residual core size (or monolayer) dispersity. The fwhm value is potentially a very sensitive measure of monodispersity. Simulations have shown<sup>6h</sup> that in disperse samples the overlapping of quantum DL charging peaks progressively reduces peak definition for peaks more removed from the MPC  $E_{PZC}$ , which is ca.  $-0.2\text{V}$ . Since the potential excursions in Figures 1 and 3 toward positive potentials are larger than toward negatives, the difference in peak definition at positive and negative potentials is thus likely due to imperfect monodispersity. (This is consistent with TEM results, below.) Another factor may be adsorption; electrode reactions of MPCs are diffusion-controlled,<sup>6g</sup> but MPCs also tend to adsorb on electrodes.<sup>3a</sup> If some of the DPV response were due to adsorbed MPCs, that response might be solvent and/or potential dependent. An additional factor could be specific adsorption of electrolyte counteranion at the monolayer/electrolyte interface, and the associated statistical distribution of MPCs with adsorbed counterions may influence the peak definition seen at positive potentials. The adsorption factors are speculative, and will require further work to clarify.

As a side point, we consider electron exchanges between MPCs diffusing to and from the electrode. This is an interesting possibility in view of the formal analogies between MPC voltammetry and electrochemical thermodynamics (i.e., eq 1) to those of redox electron transfers. The solid-state electronic conductivity of MPCs involves charge exchange between nonsolvated cores,<sup>6e</sup> electron transfers through alkanethiolate monolayers on Au surfaces are known,<sup>12</sup> and we have demonstrated<sup>6j</sup> that inter-MPC electron exchange reactions can occur in solutions between MPCs with differing charge states. The question of whether inter-MPC reactions could influence charge transport dynamics in voltammetric behavior can be gauged from the “electron diffusion coefficient,  $D_E$ ” term of the Dahms–Ruff relation<sup>13</sup>

$$D_E = k_{EX} \delta^2 C / 6 \quad (3)$$

where  $k_{EX}$  is the bimolecular ( $\text{M}^{-1} \text{s}^{-1}$ ) electron self-exchange rate constant for electron exchange, occurring at (center-to-center) distances  $\delta$  (cm) in a solution of concentration  $C$  (M). Assuming  $\delta = 2 \text{ nm}$  and  $C = 5 \times 10^{-5} \text{ M}$  (as in the present experiments), and that  $k_{EX}$  is diffusion-controlled,  $6 \times 10^9 \text{ M}^{-1} \text{ s}^{-1}$ ,  $D_E = 2 \times 10^{-9} \text{ cm}^2/\text{s}$ , which is far smaller than voltammetrically measured MPC diffusion coefficients ( $D_{PHYS} = \text{ca. } 2 \times 10^{-6} \text{ cm}^2/\text{s}$ ) (i.e., there

(11) Bard, A. J.; Faulkner, L. R. *Electrochemical Methods: Fundamentals and Applications*; John Wiley & Sons: New York, 1980; p 195.

(12) Chidsey, C. E. D. *Science* **1991**, *251*, 19–22.

(13) (a) Dahms, I. *J. Phys. Chem.* **1968**, *72*, 362. (b) Ruff, I.; Friedrich, V. *J. Phys. Chem.* **1971**, *75*, 3297.

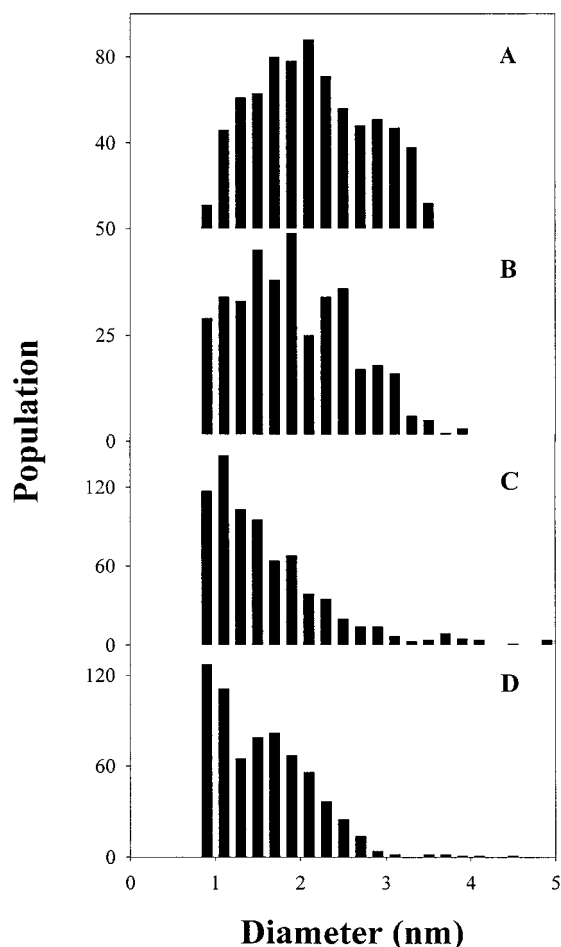


Figure 5. Transmission electron microscopy (TEM) core size histograms. (A) C6 MPC cut C (average radius  $1.0 \pm 0.28$  nm); (B) C6 MPC cut E (average radius  $1.0 \pm 0.34$  nm); (C) C8 MPC cut D (average radius  $0.7 \pm 0.22$  nm); (D) C12 MPC cut D (average radius  $0.8 \pm 0.31$  nm). The two C6 MPC samples are from different preparations.

is no charge transport effect in the present experiments). In order for the flux of inter-MPC electron transfers to influence charge transport rate currents in the voltammetry of fractionated MPCs, much higher concentrations and media in which  $D_{\text{PHYS}}$  is much smaller would be necessary.

**Evaluating MPC Core Size by Transmission Electron Microscopy (TEM).** Use of the relatively greater solubility of smaller core size MPCs in polar solvents to fractionate MPCs by the precipitation method was introduced by Whetten et al.<sup>6a</sup> and was described in the Experimental Section. TEM determination of the core size distributions of each fractionated MPC sample showed, as expected, that the average core diameter and range of measured core sizes decreased in proceeding from cut A to B to C, etc.

Examples of histograms of core diameters taken from TEM photographs are shown in Figure 5, for the more highly fractionated MPC cuts used in the DPV experiments. These histograms make the general point that while the fractionation procedure produces MPC samples sufficiently monodisperse in core size to observe quantum DL charging peaks by DPV, the monodispersity is far from perfect as measured by TEM. The DPV experiment responds to the predominant core population (the center of the

Table 3.  $^1\text{H}$  NMR Line Widths  $\nu_{\text{fwhm}}$  of MPC Methyl Peak ( $-\text{CH}_3$ )<sup>a</sup>

chain length	$\nu_{\text{fwhm}}$ cut C, Hz	$\nu_{\text{fwhm}}$ cut D, Hz
C6	51.6	37.1
C8	32.6	30.5
C10	29.5	21.1
C12	19.0	16.0

<sup>a</sup> The methyl peak appears at 0.8 ppm in the  $^1\text{H}$  NMR.  $\text{C}_6\text{D}_6$  solvent.

histogram distributions), whereas the wings of the distribution must contribute to peak broadening and the featureless background of charging currents.

Parts a and b of Figure 5 are TEM histograms of cuts C and E, respectively, obtained from two different preparations of C6 MPCs and used in the DPV experiments of Figures 1a and 3a, respectively. Both samples have *average* core diameters of 2 nm, but the size distribution in Figure 5b was more depleted in larger cores, as might be expected for a higher cut. Parts c and d of Figure 5 are cut D's of C8 and C12 MPCs, respectively. Their average diameters (Table 1) are slightly smaller than the fractionated C6 materials, apparently as a result of differences in the relative solubility contributions of core and monolayer during fractionation. It is plausible that the dispersion forces that allow solvent molecules to "feel" the core dimension of MPCs through the monolayer shell (smaller cores apparently presenting a more polar object) would be affected by the thickness of the shell. The detailed nature of these forces is unknown.

The cut D of C12 MPC shows (Figure 5d) two distinct core size populations (an effect seen before<sup>4a</sup>). One population ( $\sim 63\%$  of total) has 1.6 nm diameter cores (consistent with  $\text{Au}_{145}$  and 28 kDa mass) and the other ( $\sim 36\%$  of total) has 1 nm diameter cores (which may correspond to the truncated octahedron  $\sim \text{Au}_{116}$  or 22 kDa. The other fractionated samples probably also contain the 22 kDa material but not as sharply apparent.). Inspection of the DPV of the bimodal material in Figure 5d (shown in Figure 1c) shows that it too is discernibly bimodal, as labeled by \* and # in the figure. The former has peak spacings of 0.37 and the latter ca. 0.46 V. Using the core radii expected for 28 kDa (0.8 nm) and 22 kDa (0.6 nm) MPCs in eq 2, the predicted peak spacings are, respectively, 0.36 and 0.53 V. The agreement of experimental and theoretical  $\Delta V$  values for the minor (22 kDa) constituent of Figure 1c is reasonable given the uncertainty associated with measuring the charging peak positions in the DPV.

**Evaluating MPC Core Size by  $^1\text{H}$  NMR Spectroscopy.** We have shown previously<sup>4a</sup> that the  $^1\text{H}$  NMR  $\nu_{\text{fwhm}}$  of the methyl peak (chemical shift 0.8 ppm) of alkanethiolate ligands on MPCs varies regularly with core size. This relationship is expected from that between molecular size and  $T_2$  relaxational broadening.<sup>4a,5e</sup> The effectiveness of the precipitation fractionation procedure was tracked by NMR, and  $\nu_{\text{fwhm}}$  was found, as anticipated, to become smaller in progressive cuts. Table 3 illustrates this by comparing the methyl peak  $\nu_{\text{fwhm}}$  of cuts C and D for C6, C8, C10, and C12 MPC samples; the  $\nu_{\text{fwhm}}$  for cut D is significantly smaller in all cases. While effective at detecting changes in average core size, the NMR procedure has the disadvantage of requiring larger quantities of fractionated sample than any of the other approaches described here.

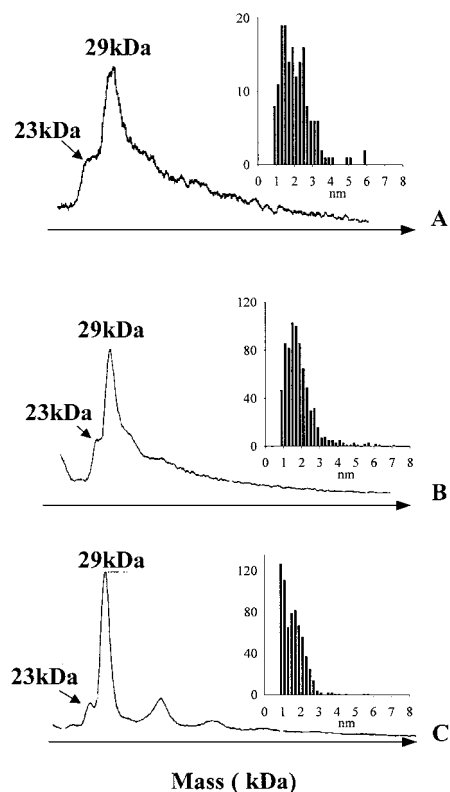


Figure 6. Laser desorption-ionization mass spectrometry (LDI/MS) of C12 Au MPCs. Insets are TEM core size histograms. (A) As-prepared C12 MPC; (B) C12 MPC cut C; (C) C12 MPC cut D. The difference of 1 kDa between 22/28 and 23/29 kDa is attributed to uncertainty in instrument calibration.

Table 3 also shows that  $\nu_{\text{fwhm}}$  decreases as the MPC chain length increases. This change cannot be simply related to MPC dimensions, since the  $\nu_{\text{fwhm}}$  value is also responding to the greater fluidity (diminished dipole-dipole broadening) experienced by methyl groups on longer chains.

**Evaluating MPC Core Size by Laser Desorption-Ionization Mass Spectrometry (LDI/MS).** Whetten and co-workers<sup>6a</sup> have shown that the LDI/MS is a very effective approach for MPC core size determination, and have used it to track the progress of fractional precipitation of C4 and C6 MPCs. LDI/MS was applied to characterize C12 MPCs in this study, as shown in Figure 6 for as-prepared, cut C, and cut D of C12 MPCs (curves A, B, and C, respectively). The LDI/MS spectra clearly show a reduction in polydispersity as fractionation proceeds and for cut D (curve C) show the bimodal MPC distribution discussed above in connection with Figures 1c and 5d.

TEM histograms are also included in Figure 6 and allow a direct comparison of the mass spectral and TEM results. The strong correlation between TEM and LDI/MS data gives a convincing picture of the success of the precipitation fractionation of C12 MPCs, which had not previously been achieved.

**Fractionating MPC Core Sizes by Extraction.** The converse of successive precipitation steps aimed at obtaining the most polar solvent-soluble (small-core) fraction of an MPC sample is to extract the as-prepared MPC sample with a polar solvent. This has been successfully done for C6 MPCs; fractionation of longer chain length MPCs such as C12 is in progress. Figure 7 compares DPV and cyclic voltammetry (CV) of solutions of C6 MPC fractionated

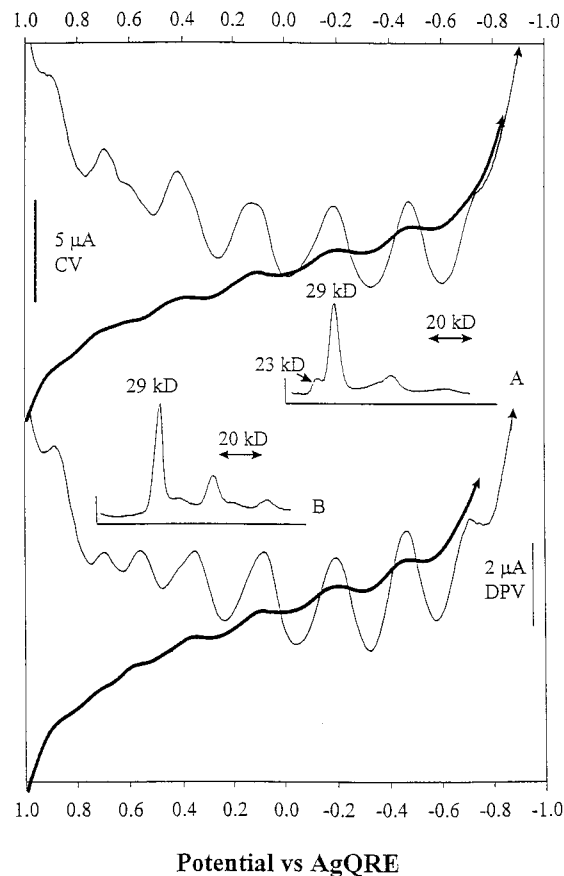


Figure 7. Positive-to-negative potential scans of differential pulse voltammogram (DPV) and cyclic voltammogram (CV) of ca. 0.1 mM C6 Au MPC in  $\text{CH}_2\text{Cl}_2$  (0.05 M  $\text{Bu}_4\text{NClO}_4$ ) at a 1.6 mm diameter Au working electrode. (A) Ethanol-soluble C6 MPC and (B) C6 MPC cut E. Insets are TEM core size histograms.

by extraction (curve A, see Experimental Section) and by precipitation (curve B, cut E). The electrochemical responses are generally similar, and Z-plots of the charging peaks give values of  $C_{\text{CLU}} = 0.55$  and  $0.62$  aF for the extracted and cut E materials, respectively.

Figure 7 (inset A) also shows an LDI/MS spectrum of the extraction-fractionated C6 sample, showing that the material is bimodal (22 and 28 kDa peaks) but otherwise comparable to precipitation-fractionated Figure 6C in being free of higher mass MPCs (unfractionated C6 MPC gives a spectrum similar to that of Figure 6A). The higher mass peaks seen in the inset are presumably gas-phase 22/28 and 28/28 dimers.

The above results show that the effectiveness of the extraction-fractionation procedure is comparable to the precipitation procedure in producing monodisperse  $\text{Au}_{145}$  (28 kDa) MPC. The extraction procedure does seem to retain a lower core size population (22 kDa) which is absent in the LDI/MS (Figure 7, inset B) spectrum of cut E C6 MPC. The clear advantage of the extraction procedure, however, is its simplicity and speed relative to the precipitation approach.

As in Figure 1c, the DPV for the ethanol-extracted MPC in Figure 7a displays some fine structure consistent with the presence of a cluster of another size in the sample. The features around 0.6 V are the most obvious evidence of this. The DPV peaks in Figure 7b show less fine structure, although it is not

entirely absent. These observations are consistent with the differences in dispersity revealed in the inset LDI/MS spectra.

In summary, the results reported show that, despite several approximations, a simple concentric sphere capacitance model is effective at representing experimental data. The significance of this result is an added confirmation of the previous<sup>6f-i</sup> interpretation of the charging peaks as electrostatic, double layer charging phenomena. Further and more refined data will undoubtedly shed light on the model's approximations.

**Comparison of Methods Summary.** This study has also provided a comparison of different approaches to measuring MPC core dispersity. The presence of DPV charging peaks, their fwhm, TEM, LDI/MS spectra, and NMR line widths are all responsive to changes in MPC dispersity produced by a series of precipitation-fractionation steps. It is worth emphasizing that these methods respond in distinctly different ways and contain subtle differences in the information provided. For example, the DPV response is, strictly speaking, to the value of and dispersity in cluster capacitance,  $C_{CLU}$ , whereas TEM responds to the scattering diameter of the MPC core, and LDI/MS to a complex desorption-  
ionization process in which most ligands are lost. The DPV experiment thus responds to any dispersity in the MPC monolayer as well as in the core, whereas the other two methods respond differentially to the core. Whether significant dispersity in the monolayer shell from MPC to MPC exists is unknown; the

generally good agreement between DPV, TEM, and LDI/MS seen here suggests that it is not large, at least.

The value of convenient experimental measures of MPC dispersity should be obvious; to investigate relationships between the core dimension and chemical reactivity (such as in place-exchange reactions<sup>3a,b</sup>) and other properties, monodisperse samples must be prepared. Procedures discussed here are suitable (if arduous) for preparing moderately monodisperse MPCs with alkanethiolate ligands. Comparable procedures for MPCs with functionalized monolayer shells remain to be worked out.

#### ACKNOWLEDGMENT

This work was supported in part by grants from the National Science Foundation and the Office of Naval Research. A.C.T. acknowledges support from Dobbins and Lord Corporation Fellowships.

#### SUPPORTING INFORMATION AVAILABLE

Differential pulse voltammogram and Z plot for C16 MPC (3 pages). This material is available free of charge via the Internet at <http://pubs.acs.org>.

Received for review April 23, 1999. Accepted July 1, 1999.  
AC990432W